

<https://doi.org/10.1038/s44310-025-00062-9>

# Observation of nonlinear input-output power characteristic of light emission from an electrically-biased metallic photonic crystal

Check for updates

Mei-Li Hsieh<sup>1,2</sup>, Tyler Romero<sup>1</sup>, J. A. Bur<sup>1</sup>, Xuanjie Wang<sup>3</sup>, Jih-Sheng Wu<sup>2</sup>, Shankar Narayan<sup>3</sup>, Sajeev John<sup>4</sup> & Shawn-Yu Lin<sup>1,2</sup>✉

We report, to the best of our knowledge, the first realization of an electrically-biased, resonant-cavity metallic photonic-crystal (PC) emitter. The PC device is electrically-biased and is driven out of thermal equilibrium. The PC emission exhibits a strongly nonlinear input-output power characteristic at the resonant peak wavelength,  $\lambda \sim 1.7 \mu\text{m}$ . Particularly, at lower bias, the emission power shows an exponential growth over 3 orders-of-magnitude. At higher bias, the growth slows down and shows a linear dependence on input power. This observed output/input characteristic may arise from non-equilibrium injection of hot electrons, the excitation of localized surface plasmons at the interior surfaces of the PC and photon emission to optical passband modes of the PC/ resonant cavity structure.

Thermal radiation of a metallic object has been a subject of great interest since the pioneering work of M. Planck<sup>1</sup>. Recently, thermal radiation modification by complex photonic-crystal (PC) structures<sup>2–6</sup> has attracted attention due to its potential energy applications in thermo-photovoltaics<sup>7–10</sup> and tunable infrared light sources. Planck's Law of thermal radiation successfully predicts the broadband emission spectrum of a hot object under equilibrium<sup>1</sup>. Planck's Law also sets the upper limit of radiation intensity at any given temperature (T) and wavelength ( $\lambda$ ). Recently, some intriguing experiments show that radiation from a metallic PC can deviate from the Planck's Law in the far-field, i.e. non-Planckian behavior<sup>11,12</sup>. For example, the metallic PC radiation can have a narrow band characteristic and its peak intensity exceeds the blackbody (BB) limit at the resonant frequencies. Furthermore, the metallic PC radiation can exhibit a large optical non-reciprocity<sup>13</sup>, indicative of a non-equilibrium process. In 2004, it was shown that the observed non-Planckian behavior<sup>8,11,12</sup> cannot be explained classically under equilibrium assumption<sup>14</sup>, where the calculation treats the emitting source as a random fluctuating current. Subsequently, in 2006–2007, two independent quantum mechanical pictures of thermal radiation from a metallic PC were proposed<sup>15,16</sup>. Both formulations suggest the occurrence of non-Planckian radiation under non-equilibrium conditions. The paper by Kaso and John further predicts the occurrence of optical nonlinearity, i.e. a nonlinear input-to-output power characteristic from a

metallic PC<sup>16,17</sup>. To confirm the intriguing non-equilibrium, nonlinear behavior and to obtain an accurate measurement of the input and output power, we build an electrically-biased metallic PC device.

In this paper, we report the realization of an electrically-biased tungsten (W) PC light-emitting device. An electrical biased scheme makes it possible to introduce hot electrons directly to the tungsten filament, providing slight non-equilibrium excitation to the light-emitting filament. An electrical-biased W-PC device is also easier to operate through a direct current injection<sup>18</sup>. In this work, we performed DC bias of the W-PC device at a series of input power and measure its emitted radiation spectra and output power. The measured output power at resonant wavelength regime,  $\lambda \sim 1.7 \mu\text{m}$ , is found to increase nonlinearly and even exponentially versus the input electrical power. The observed nonlinearity in the input-output power characteristic of our W-PC device may arise from the injection of hot electrons<sup>19–21</sup>, the excitation of localized surface plasmons<sup>20–23</sup> at the interior surfaces of our W-PC structure and, finally, photon emission to optical passband modes of the PC/ resonant-cavity structure<sup>16,17</sup>.

## Results

### Sample and device fabrication

The sample structure used in this experiment has been reported earlier<sup>11,24</sup>. Briefly, it consists of a micro-cavity fabricated on top of a 3D tungsten-PC

<sup>1</sup>The Department of Physics, Applied Physics and Astronomy, Rensselaer Polytechnic Institute, Troy, NY, 12180, USA. <sup>2</sup>The Department of Photonics, National Yang Ming Chiao Tung University, Hsinchu, Taiwan. <sup>3</sup>The Department of Mechanical, Aerospace and Nuclear Engineering, Rensselaer Polytechnic Institute, Troy, NY, 12180, USA. <sup>4</sup>The Department of Physics, University of Toronto, Toronto, Ontario, Canada. ✉e-mail: [sylin@rpi.edu](mailto:sylin@rpi.edu)

(W-PC) on a four-inch silicon wafer. The PC-cavity structure has a cavity resonance at  $\lambda \sim 1.7 \mu\text{m}$ . The resonant mode functions as an isolated optical passband for photon emission<sup>11,16</sup>. The micro-cavity is formed by a SiO<sub>2</sub> layer of thickness  $t_{\text{cav}} = 554 \text{ nm}$  sandwiched on both sides by SiO<sub>2</sub>/Si Distributed Bragg Reflector (DBR) mirrors. The thicknesses of the SiO<sub>2</sub> and Si are  $t_{\text{oxide}} = 275 \text{ nm}$  and  $t_{\text{Si}} = 120 \text{ nm}$ , respectively. The 3D W-PC has diamond lattice symmetry<sup>25</sup> and consists of six layers of alternating one-dimensional tungsten-rods<sup>24</sup>. The 1D tungsten-rods have a height of  $h = 0.6 \mu\text{m}$ , a rod width of  $w = 0.5 \mu\text{m}$  and a rod-to-rod spacing of  $a = 1.5 \mu\text{m}$ . The 3D W-PC is fabricated using standard micro-electronic processing. It is built by the repetitive deposition and etching of multiple dielectric and tungsten films. To accomplish this goal, a comprehensive six-level stacking process was developed. Within each layer, SiO<sub>2</sub> was first deposited, patterned and etched. The resulting trenches were filled with tungsten and the surface of the wafers were made flat using chemical mechanical polishing. Before electrical testing, the microcavity W-PC sample is diced into  $\sim 2.5 \times 10 \text{ mm}^2$  long stripe and the silicon substrate thinned down to  $\sim 100 \mu\text{m}$ . To allow for electrical contact, tungsten PC layers were exposed by conducting selective dry-etching through the top SiO<sub>2</sub>/Si DBR layers. The advantage of the dry etching approach is that W-PC sample is supported by a  $\sim 100 \mu\text{m}$  thick silicon substrate and easier to handle.

**Experimental testing setup**

Figure 1a shows a schematic of an electrically biased W-PC light-emission-device. Electric contacts were made directly on top of the exposed W-PC layers. This way, electrical current can be injected directly to the interconnected tungsten PC-layers. When the injected current is increased, voltage across the contacts is increases and so is the injected electrical power ( $P_{\text{IN}}$ ). As a result, radiation through the top device surface (the red arrows) is expected to increase. Figure 1b shows a photo of the W-PC sample with  $100 \mu\text{m}$  silicon substrate. It is mounted to Ni ribbon contact pads, blazed into a homemade Alumina ceramic mounting stage. The Alumina mount is thermally insulating so as to reduce thermal conduction loss and it is also electrically insulating. For temperature monitoring purpose, a thermal couple is mounted to the side and near the top of the Ni contact pad. Figure 1c shows a COMSOL computed temperature profile of the sample, Ni pad and ceramic mount for  $P_{\text{IN}} = 4 \text{ Watts}$ . We notice that temperature gradient exists across the  $10 \text{ mm}$  long sample and, therefore, the sample is not strictly in thermal equilibrium. The average sample temperature is  $\langle T_1 \rangle = 590 \text{ K}$  at  $P_{\text{IN}} = 4 \text{ Watts}$ . The highest  $T$  occurs at the middle position (red color) and is  $T_1 = 620 \text{ K}$ . And the temperature at the thermal-couple position near the top of the contact pads is  $T_2 = 466 \text{ K}$ . At the moment, it is not possible to measure the sample’s surface temperature directly by either using a light-weight thermal couple or an IR camera<sup>11,13</sup>. A similar challenge encountered in the measurement of waveguide core has also been reported<sup>26</sup>. However, a COMSOL model calculation<sup>11,12</sup> can provide a reasonable estimation of the sample’s surface temperature profile. For example, we can check if the model is realistic by comparing the calculated and measured temperatures at the thermal-couple position ( $T_2$ ) for a series of input power ( $P_{\text{IN}}$ ). Table 1 shows a summary of the calculated and measured  $T_2$  temperatures, which agrees with each other within  $11^\circ$ . The COMSOL model detail is described in the METHOD section. Figure 1d shows a SEM image of the 3D Tungsten-PC, integrated with the Si/SiO<sub>2</sub> microcavity structure. Next, we present spectroscopy study of light emission from our electrically-biased PC devices. For comparison purpose, light emission from a thermally-excited PC device is also shown.

Figure 2a shows the measured reflectance spectrum of our W-PC sample. The high reflectance ( $R > 0.95$ ) occurs over  $\lambda = 1.35\text{--}2.4 \mu\text{m}$ , corresponding to the Distributed-Bragg-Reflector (DBR) stop band regime. The pronounce reflectance dip at  $\lambda \sim 1.7 \mu\text{m}$  is due to the fundamental cavity resonance of our W-PC structure. It has a spectral full-width-half-maximum (FWHM) of  $50 \text{ nm}$ . The broader reflectance dip at  $\lambda \sim 1.15 \mu\text{m}$  is due to the band edge resonance, having a linewidth FWHM  $\sim 110 \text{ nm}$ . In Fig. 2b, c, we show the spectral radiance of a thermally-excited and an electrically-biased W-PC sample, respectively. Figure 2b shows radiance

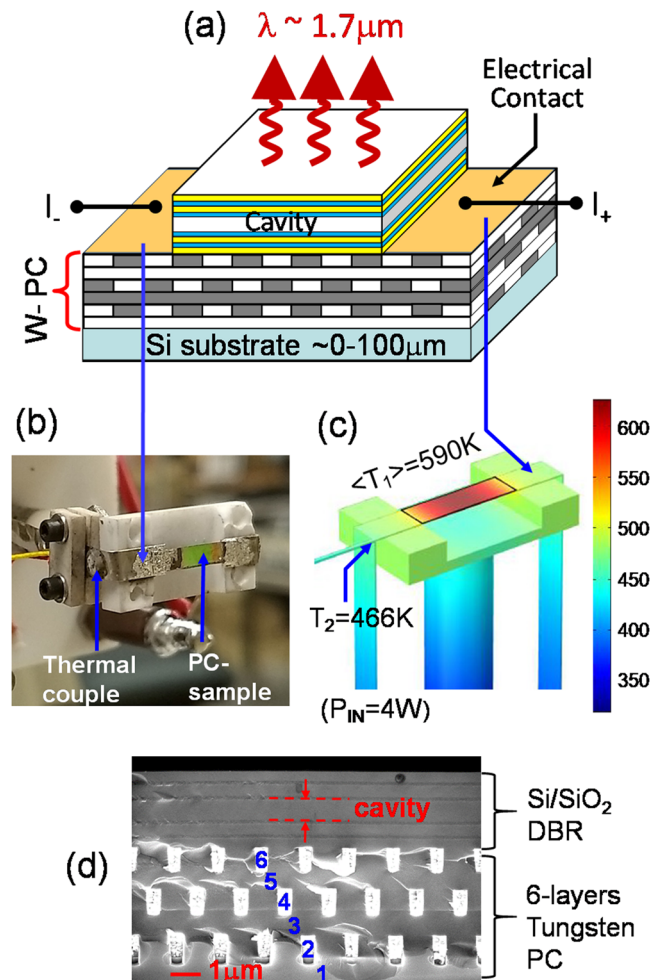


**Fig. 1 | The electrically biased sample structure, sample mounting scheme and a calculated temperature profile.** **a** A schematic of an electrically biased PC light-emission-device. Electrical current is injected directly to the metallic photonic crystal to excite localized surface plasmons. **b** A photo of the W-PC sample mounted to Ni contact wires and is supported by an Alumina ceramic mount. **c** A COMSOL computed temperature profile of the PC sample, Ni-contact pad and ceramic mount for  $P_{\text{IN}} = 4 \text{ Watts}$ . **d** A SEM image of the 3D Tungsten-PC and Si/SiO<sub>2</sub> DBR (Distributed Bragg Reflector) micro-cavity structures.

**Table 1 | Measured and Calculated T**

$I_{\text{IN}}$ (A)	$P_{\text{IN}}$ (W)	$T_2$ (t.c.)_ Experiment	$T_2$ (t.c.)_ Calculation	$\langle T_1 \rangle$ _ Calculation
1.875	3.2 W	454 K	443 K	549 K
2.00	4.0 W	470 K	466 K	590 K
2.075	5.1 W	492 K	498 K	654 K

data of the thermally excited sample (i.e. sample heated by a thermal heater<sup>12</sup>) taken at three temperatures:  $T = 633, 683$  and  $723 \text{ K}$ . Note that the method for determining the absolute spectral radiance has been presented earlier<sup>13</sup>. For reference purpose, the spectral radiance of a blackbody (BB) is also shown. We would like to make three points. **First**, the W-PC radiation (the black curve) exhibits a peak-emission at  $\lambda \sim 1.7 \mu\text{m}$ . As  $T$  is increased from  $T = 633$  to  $723 \text{ K}$ , the peak-radiance increases accordingly. However, the peak-wavelength is pinned at  $\lambda \sim 1.7 \mu\text{m}$ . This is in sharp contrast to that predicted by Wien’s displacement law for an equilibrium thermal radiation<sup>27</sup>. **Secondly**, we note that the peak-wavelength matches the fundamental cavity reflectance dip, shown in Fig. 2a. This agreement indicates that the photon emission arises from the influence of the underlining

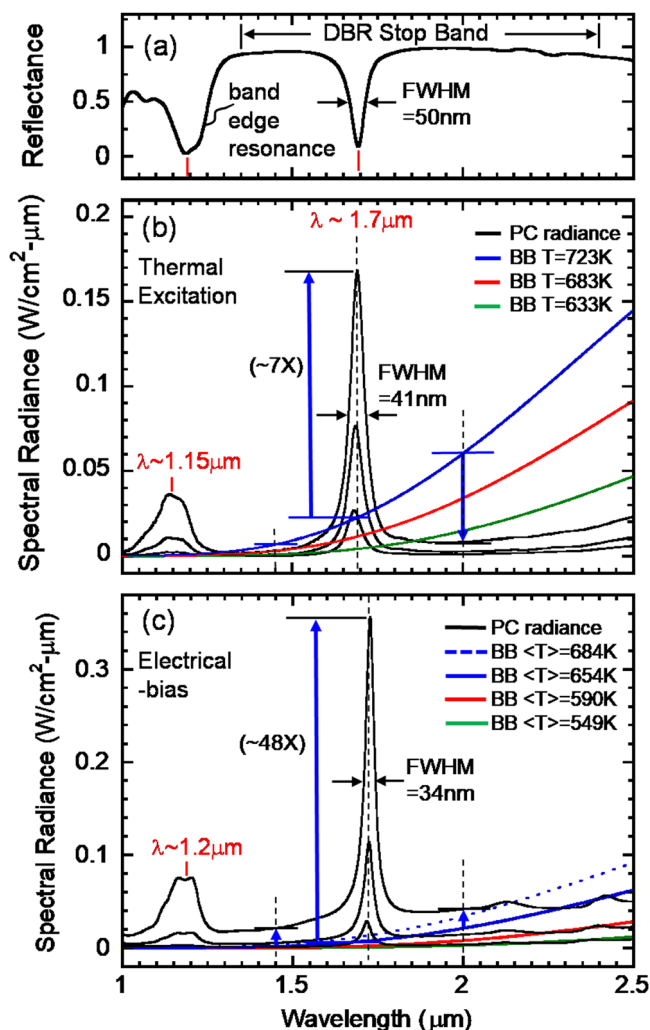


**Fig. 2 | The measured reflectance spectrum and radiation spectra for both thermally and electrically biased cases.** **a** The measured reflectance spectrum of our W-PC sample with a  $\sim 100 \mu\text{m}$  thick silicon substrate. **b** The measured spectral radiance of a thermally excited PC-sample, taken at three sample temperatures:  $T = 633, 683$  and  $723 \text{ K}$ . **c** The spectral radiance of an electrically biased W-PC, taken at three input power,  $P_{\text{IN}} = 3.2, 4.0$  and  $5.1 \text{ Watts}$ .

resonant cavity W-PC band structure. Also, the peak-emission linewidth is  $\text{FWHM} = 41 \text{ nm}$ , which is slightly narrower than that of the cold cavity  $\text{FWHM} = 50 \text{ nm}$ . **Thirdly**, we compare the spectral radiance of our W-PC to that of a blackbody (the blue curve) at  $T = 723 \text{ K}$ . At off-the-resonance, e.g.  $\lambda = 1.45$  and  $2 \mu\text{m}$ , the W-PC radiance is weaker than the BB one by  $\sim 3$  and  $5$  times (the downward blue arrow), respectively. Yet, on resonance at  $\lambda \sim 1.7 \mu\text{m}$ , the W-PC radiance is  $7$  times stronger than the BB radiance (the upward blue arrow). Here, we observe a simultaneous enhancement/ suppression of radiation on and off the resonant mode at  $\lambda \sim 1.7 \mu\text{m}$ . This finding seems to suggest a spectral redistribution of thermal radiation energy on and off-the-resonance in our W-PC sample. So, thermal radiation at off-the-resonance regime is suppressed by the DBR stop-band, leading to a redistribution of energy into the resonant-mode regime. At the resonance, the  $7$ -times enhancement of W-PC radiance over BB further indicates that the sample’s emission process is non-equilibrium<sup>15</sup>. A similar behavior of energy redistribution holds true for data taken at the other two temperatures,  $T = 683$  and  $633 \text{ K}$ . Next, we examine PC radiation data taken from an electrically-biased device.

Figure 2c shows spectral radiance of an electrically biased W-PC, taken at three input power,  $P_{\text{IN}} = 3.2, 4.0$  and  $5.1 \text{ Watts}$ . The corresponding measured and calculated temperatures at the thermal coupled position are

$T_2^{\text{measure}} = 454, 470, 492 \text{ K}$ , and  $T_2^{\text{cal}} = 443, 466, 498 \text{ K}$ , respectively. These two sets of temperature agree with each other within  $11 \text{ K}$ . Also, the sample’s average temperature, calculated from COMSOL model, are  $\langle T_1 \rangle = 549, 590$  and  $654 \text{ K}$ , respectively. Similar to the thermal-excited sample case, the electrically-biased sample has a peak-radiance at  $\lambda \sim 1.7 \mu\text{m}$ . Nonetheless, its spectral linewidth is narrower,  $\text{FWHM} = 34 \text{ nm}$ , than either the thermal-excitation case of  $\text{FWHM} = 41 \text{ nm}$  or the cold-cavity case of  $\text{FWHM} = 50 \text{ nm}$ . We now compare the PC and BB spectral radiance (the blue curve) at  $\langle T_1 \rangle = 654 \text{ K}$ . At off-the-resonance regime, the W-PC radiance is  $\sim 2$  times higher (the upward blue arrow) than the BB one at  $\lambda = 2 \mu\text{m}$  and  $\sim 12$  times higher at  $\lambda = 1.45 \mu\text{m}$ . This finding is contrary to that observed in the thermal-excitation case. Furthermore, on resonance at  $\lambda = 1.72 \mu\text{m}$ , the W-PC radiance is  $\sim 48$  times higher than the BB radiance. This observation shows that the W-PC emission is strongly enhanced on-resonance and also weakly enhanced at off-the-resonance regime. Note that this comparison makes sense only if the sample temperature is accurate and, particularly, not under-estimated. At the moment, there is no good way to place a temperature probe on the sample surface, without disturbing its surface temperature. However, from COMSOL calculation, the highest surface  $T$  occurs at the middle section of the sample and reads  $T = 684 \text{ K}$  at  $P_{\text{IN}} = 5.1 \text{ Watts}$ . For reference purpose, the BB spectral radiance at  $T = 684 \text{ K}$  is also plotted (the blue dotted curve). Comparing to the BB radiance at  $T = 684 \text{ K}$ , the W-PC radiance is still  $6x, 28x$  and  $1.2x$  higher than the BB radiance at  $\lambda = 1.45, 1.72$  and  $2 \mu\text{m}$ , respectively. Similar findings hold true for W-PC radiance taken at  $\langle T_1 \rangle = 654$  and  $590 \text{ K}$ , respectively. As the sample temperature is not well-defined in our electrical-bias case, the observed enhancement of radiation power over that of a blackbody is not termed “super-Planckian” for our electrically biased PC device. Also, this observation suggests that the picture of thermal energy redistribution is not valid in the case of electrically-biased configuration. Especially, the strong photon emission at the resonance might not be dominated by thermal heating of the W-PC sample, but rather, by other excitation mechanisms relating to the nature of electrical current injection.

Figure 3 summarizes the ratio of the PC- and BB-spectral radiance, where the ratio is defined as: PC radiance ( $\lambda, T$ ) / BB radiance ( $\lambda, T$ ). Ordinarily, in the case of thermal equilibrium, the ratio is called spectral “emissivity”. However, since the heated W-PC device is not under equilibrium condition and the temperature of the W-PC sample is not uniform across the sample, so we called it the “effective emissivity”. Figure 3a shows the effective emissivity of the thermally excited W-PC sample. The blue dashed line indicates “unity” ratio and is the blackbody limit. Again the peak resonance occurs at  $\lambda \sim 1.7 \mu\text{m}$ . The peak position shows a slight red shift from  $\lambda = 1.681, 1.686$  to  $1.690 \mu\text{m}$  as temperature is increased from  $T = 633, 683$  and  $723 \text{ K}$ , respectively. On resonance, the ratio is  $\sim 7$  times ( $700\%$ ) higher, indicating an enhanced emission. At off-the-resonance regime, the ratio is less than one which indicates a suppressed emission. As mentioned earlier, our PC emission is under the influence of the 3D W-PC band structure and has a more directional emission<sup>28</sup>. This directional emission may contribute to about  $60\%$  emission enhancement at  $\lambda \sim 1.7 \mu\text{m}$ . So, out of the  $700\%$  enhancement, about  $60\%$  of it is from directional consideration of PC structure and the rest from energy redistribution into the resonant mode. Figure 3b shows the effective emissivity of the electrically-biased W-PC sample. Again, the blue dashed line indicates “unity” ratio. The peak position also shows a slight red shift from  $\lambda = 1.717, 1.722$  to  $1.726 \mu\text{m}$  as  $T$  is increased from  $549, 590$  and  $654 \text{ K}$ , respectively. On resonant peak, the ratio is  $\sim 48$  times higher, indicating a large enhancement of emission. Off the resonance and at the longer- $\lambda$  regime (e.g.  $\lambda = 2 \mu\text{m}$ ), the ratio is slightly higher than one and starts to approach the BB limit. Off the resonance and at the shorter- $\lambda$  regime (e.g.  $\lambda = 1.4-1.5 \mu\text{m}$ ), the ratio is  $6-10$  and shows a larger deviation from the BB limit. This deviation may be due to fact that it is in the vicinity of another band edge resonance at  $\lambda \sim 1.2 \mu\text{m}$ . To conclude, we note that the picture of modification of thermal radiation makes sense for the thermally-excited PC device. This is when the W-PC sample is heated thermally by a heating filament (thermal bath). And, the W-PC sample and the heating filament is in close contact and under quasi-equilibrium

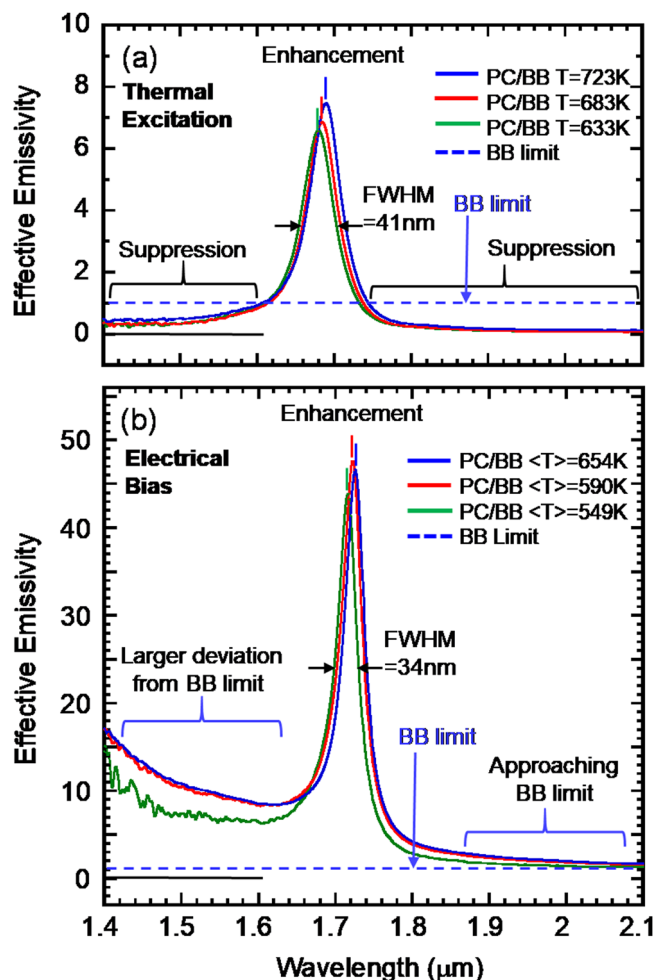


**Fig. 3** | A summary of the ratio of spectral radiance between our PC and the BB, where the ratio is defined as: PC radiance ( $\lambda, T$ ) / BB radiance ( $\lambda, T$ ). **a** The radiance ratio of the thermally excited PC device. The blue dashed line indicates “unity” ratio and is the blackbody limit. **b** The radiance ratio of the electrically biased PC device. Again, the blue dashed line indicates “unity” ratio.

condition. However, for the electrically-biased W-PC sample, the picture of thermal radiation modification may not apply. This is evident from the W-PC emission enhancement over broad wavelength regime (a large enhancement on resonance at  $\lambda \sim 1.7 \mu\text{m}$  and an intermediate enhancement off-the-resonance) and also over a wide temperature range ( $T = 549\text{--}654 \text{ K}$ ).

To illustrate the non-equilibrium nature of our observed W-PC radiation, in Fig. 4, we summarize the peak spectral radiance versus temperature for the thermally-excited (blue dots) and electrically-biased (red squares) W-PC sample. The blackbody radiance (black dots) at  $\lambda = 1.7 \mu\text{m}$  is also shown for reference purpose. When the W-PC sample is thermally excited, its peak radiance is higher than the BB radiance by a moderate 6–7 times for temperature ranging from  $T = 510\text{--}700 \text{ K}$ . This data shows that, under thermal excitation, W-PC radiation deviates from the typically BB behavior in equilibrium. As reported earlier, the source of non-equilibrium might come from the heating filament (heat bath), which has a slightly higher temperature than the W-PC’s surface temperature<sup>12</sup>. Furthermore, when the W-PC sample is electrically biased, its peak radiance is higher than the BB radiance by 30–50 times for  $T = 500\text{--}700 \text{ K}$ . So, under electrical excitation, W-PC peak radiation deviates much more significantly from the typical BB behavior. And so, for the electrically biased case, temperature might not be a good parameter to characterize the status of energy excitation. From the spectral characteristics shown in Figs. 2 and 3, and from the temperature

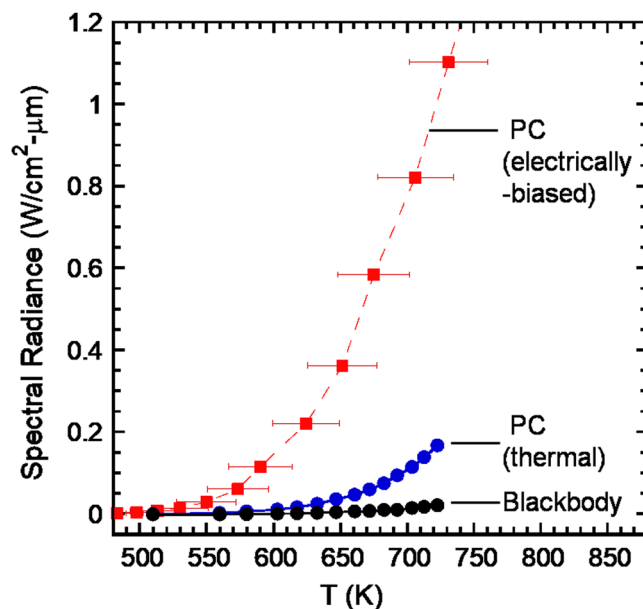
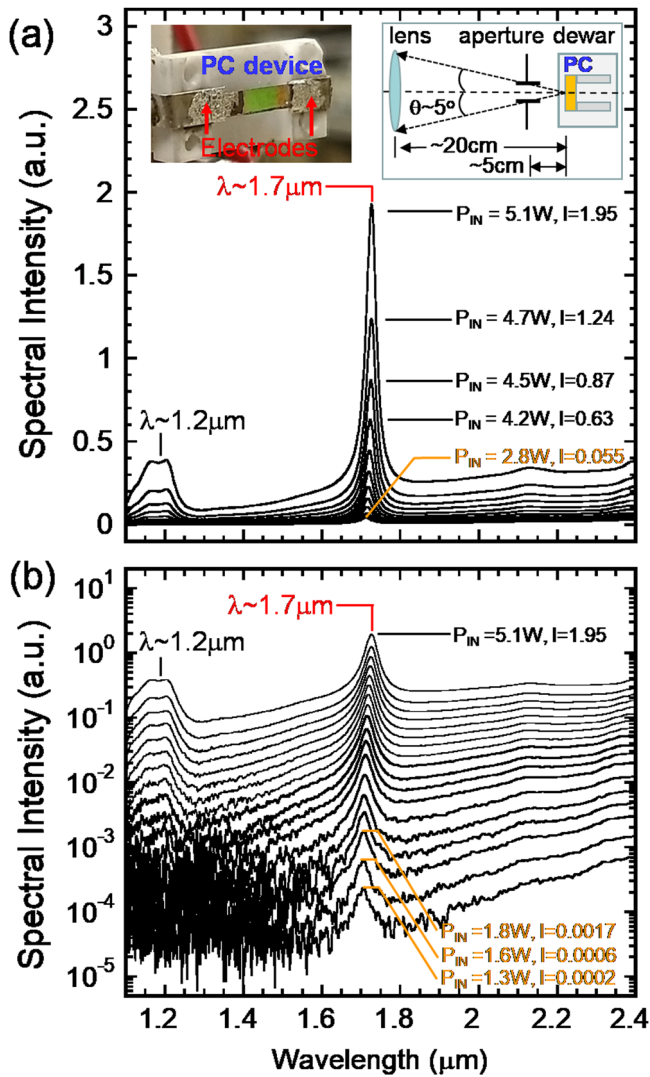


**Fig. 4** | A comparison of the peak spectral radiance versus temperature for the thermally excited (blue dots), the electrically biased (red squares) PC sample and the blackbody (black dots) at  $\lambda = 1.7 \mu\text{m}$ .

dependence shown in Fig. 4, we may conclude that the observed W-PC radiation exhibits significant deviation from the standard, equilibrium BB spectral behavior. To further illustrate such a non-equilibrium behavior, we will next show a systematic study of W-PC emission over a larger biased range. Also, instead of examining the “radiance versus temperature” relationship, we will next study the “ $P_{\text{IN}}$ -versus- $P_{\text{OUT}}$ ” dependence of the electrically biased W-PC sample.

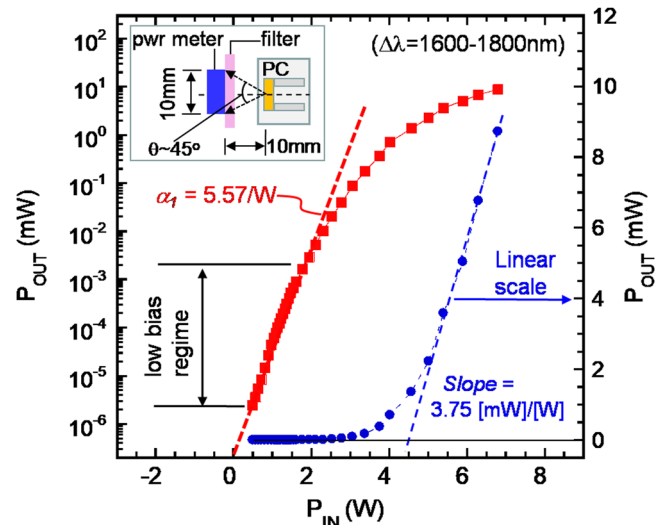
Figure 5 shows the measured radiation spectra of an electrically biased W-PC device for input power ranging from  $P_{\text{IN}} = 1.3\text{--}5.1 \text{ W}$ . The spectra are taken using a FTIR spectrometer in the near-infrared wavelength. Figure 5a shows the spectral plot in a linear scale for  $P_{\text{IN}} = 2.8\text{--}5.1 \text{ W}$ . The inset (to the left) shows a photo of the mounted W-PC device. The inset, to the right, shows a schematic of the optics to collect radiation from inside the optical dewar to the FTIR spectrometer. When the input power is increased from  $P_{\text{IN}} = 2.8\text{--}5.1 \text{ W}$ , the corresponding peak spectral intensity (arbitrary unit) increases rapidly from  $I = 0.055$  to 1.95. Hence, when  $P_{\text{IN}}$  is increased by less than 2 times, the corresponding output intensity is increased by ~40 times. This data illustrates the occurrence of a strongly non-linear input-output intensity characteristic in our W-PC device. To better resolve the low intensity data and to further illustrate the non-linearity, in Fig. 5b, we plot the spectra in a semi-logarithmic scale. In this plot, the emission spectrum at  $P_{\text{IN}} = 1.3 \text{ W}$  can be resolved and the peak intensity is as low as  $I = 0.0002$ . This time, when the input power is increased from  $P_{\text{IN}} = 1.3\text{--}5.1 \text{ W}$ , the output optical power is increased from  $I = 0.0002$  to 1.95. So, while  $P_{\text{IN}}$  is increased by about 4 times, the corresponding output optical power is increased by ~10,000 times, or 4 order-of-magnitudes. This data demonstrates a strong optical non-linearity taken place in our electrically biased PC light emitter.

Figure 6 summarizes the power-in versus power-out characteristic of our W-PC sample at the peak emission regime in both the linear (blue dots) and logarithmic (red squares) scales. The inset shows a schematic of the optics to collect optical radiation. Given that W-PC emission is directional to within  $\pm 20^\circ$ <sup>28</sup>, this collection optics is sufficient to collect all the emitted power from the W-PC sample. The optical power is obtained using a calibrated power meter, having a detecting size of  $10 \times 10 \text{ mm}^2$ <sup>27,9</sup>. The bandpass filter is placed in front of the power meter to allow power collection over the emission regime,  $\Delta\lambda = 1600\text{--}1800 \text{ nm}$ . The bandwidth of  $\Delta\lambda = 200 \text{ nm}$  is narrow enough to eliminate any unwanted radiation from the optical dewar and the background. Yet, it is wide enough to collect power over the entire



**Fig. 5 | Spectral intensity of light emission at a series of electrical bias-current (I).** a Radiation spectrum of an electrically biased PC sample, plotted in a linear scale. The input electrical power is from  $P_{IN} = 2.8$  W to 5.1 W. b The same radiation intensity spectrum, plotted in a semi-logarithmic scale for  $P_{IN} = 1.3$  W to 5.1 W. The radiation intensity at  $\lambda = 1.7$   $\mu\text{m}$  increases by four-order-of-magnitudes (from  $2 \times 10^{-4}$  to 1.95) when  $P_{IN}$  is increased by only four times, i.e. from  $P_{IN} = 1.3$  W to 5.1 W.

peak spectral regime for all biases,  $P_{IN} = 1.3\text{W} - 5.1$  W. In the linear plot (blue dots), the output power shows an initial quick turn-on at low input power and then a linear growth at higher input power,  $P_{IN} > 5$  W. The linear dependence at high input power regime yields a slope:  $S \equiv \Delta P_{OUT}(\text{mW}) / \Delta P_{IN}(\text{W}) = 3.75$ . In the semi-log plot (red squares),  $P_{OUT}$  shows an initial exponential growth over 3 order-of-magnitudes (the straight, red dotted line) at low input powers,  $0 < P_{IN} < 2$  W. The exponential dependence is fitted to an empirical function:  $y = Q_0 \times e^{\alpha_1 x}$ . Here, “y” and “x” represent the input ( $P_{IN}$ ) and output ( $P_{OUT}$ ) powers, respectively. From the fitting, we find  $Q_0(\text{mW}) \cong 1.0 \times 10^{-7}$  and  $\alpha_1 \cong 5.57 \text{ W}^{-1}$ , respectively. An exponential dependence in the  $P_{IN}$ -versus- $P_{OUT}$  relationship is indicative of optical gain in the emitted radiation. It may arise from hot electrons injection into upper energy levels of the W or W-oxide nano-dots, which are randomly distributed at the interior surface of W-PC structure. Subsequently, those hot electrons could make transition into lower energy levels and produce radiation into the passband mode at  $\lambda \sim 1700$  nm. At higher input power,  $P_{IN} > 5$  W, the exponential growth slows down and the dependence becomes linear. This may be due the occurrence of additional loss mechanism such as a stronger electron-phonon coupling, when the sample



**Fig. 6 | The optical output power ( $P_{OUT}$ ) versus electrical input power ( $P_{IN}$ ) characteristic of an electrically biased PC sample.** The data is plotted in a linear-scale (blue dots) and also a logarithmic scale (red dots). While  $P_{IN}$  is increased by  $\sim 13$  times (from 0.5 W to 6.6 W),  $P_{OUT}$  is increased by  $\sim 10$  million times (i.e. from  $\sim 1$  nW–10 mW).

is under higher bias and at higher average temperatures. Additionally, from Fig. 6, we note the output radiation power at  $\lambda = 1600 - 1800$  nm for our device is relatively low as compared to the input electrical power. In the future, this may be improved by reducing the device’s thermal mass by removing the thick 100  $\mu\text{m}$  silicon substrate and leaving behind only the cavity/W-PC thin film of  $\sim 4$   $\mu\text{m}$  thick.

### Discussion

A possible explanation of the observed optical non-linearity in a cavity-PC structure may be found in a 2007 theoretical paper by Kaso and John<sup>16</sup>. The stated criteria are: (I) the occurrence of an isolated passband in the structure; (II) the existence of nonlinear oscillators; and (III) the system is under external, non-equilibrium pumping. In our cavity-PC sample structure, the  $\lambda \sim 1.7$   $\mu\text{m}$  resonance acts as an isolated optical passband for photon emission. Also, in our sample, inhomogeneously broadened nonlinear oscillators<sup>16</sup> may arise from discrete energy levels of the W and/ or W-oxide nano-dots<sup>19–23</sup> due to rough tungsten surface of the W-PC structure<sup>28</sup>. With a sufficient density of non-linear oscillators coupled to LSR and under external pumping, Kaso and John theoretically found that non-linear Bloch waves can be excited within the passband of the metallic PC and exhibits a laser-like input pumping and output amplitude characteristic<sup>16</sup>. The photonic-crystal band effects and PC passband mode play a crucial role in these observations by providing optical feedback. This is the most novel aspect of the overall process. Hot electrons and plasmonic resonances are how the photonic crystal modes are pumped with photons to eventually cause stimulated emission. Our experimental observation provides for a direct evidence of a non-linear response from an externally pumped 3D W-PC structure.

In summary, we report the successful realization of an electrically-biased W-PC light emitter. The emission is under the influence of the underlining cavity W-PC structure, is a non-equilibrium emission and exhibits a strongly nonlinear output/input power characteristic at  $\lambda \sim 1.7$   $\mu\text{m}$  peak emission wavelength. At low input power regime, the output/input relationship shows an exponential dependence over three orders-of-magnitude. At higher input power, the exponential growth of output power slows down and the output/input curve shows a linear dependence. This study demonstrates, for the first time, a non-equilibrium and nonlinear light emission from an electrically-biased W-PC emitter. It is

a remarkable observation that, unlike standard thermal emitter, our photonic-crystal emitter can exhibit qualitatively different behavior with small deviations from equilibrium.

## Methods

### Methods for Thermal Flow Modeling

COMSOL Multiphysics software (version 5.2a) was used to compute the temperature distribution across the sample. Because the device contains features with dimensions of different scale (i.e. W-rods with a width = 500 nm, and a total W-PC sample size of  $\sim 3 \times 10 \text{ mm}^2$ ), the computation is performed in two parts. The first part simulates a  $70 \times 70 \mu\text{m}^2$  section of the Si/SiO<sub>2</sub> DBR (Distributed Bragg Reflector) and W-PC on the silicon substrate using a finer mesh to accommodate a minimum feature size of 500 nm. The thermophysical properties of different materials (Si, SiO<sub>2</sub>, W), such as thermal conductivity, densities, heat capacity, electrical conductivity and emissivity, were obtained from the built-in database of the COMSOL software. Also, the thermal contact resistance between adjacent layers is considered negligible compared to the bulk thermal resistance of the corresponding layers. Since this is a three-dimensional model, it considers any thermal spreading or constriction resistance. The second part of the computation includes the 100  $\mu\text{m}$ -thick silicon substrate, the Ni bonding pads, and the Alumina ceramic sample mount, assuming a sample area of  $3 \times 10 \text{ mm}^2$ . This is accomplished using the Joule heating module in the COMSOL software. Here, the PC filament resistance is set to be 1 ohm. The Ni lead thickness 0.15 mm, with a Ni emissivity of 0.6, and a ceramic emissivity of 0.10 and the applied voltage varied from 1–2.26 Volts. The radiation loss through the sample surfaces is given by the Stefan-Boltzmann Law:  $M_e = \epsilon \sigma_e T$ , where  $\epsilon$  is the material emissivity and  $\sigma_e = 5.67 \times 10^{-12} \text{ watt}/(\text{cm}^2 \text{K}^4)$  is the Stefan-Boltzmann constant. The dominant conduction loss is due to heat flow from the hot metallic PC-filament through its electrical contacts to the room-temperature sample mount assembly/dewar. To simplify the modeling, the sample mount/dewar is treated as a thick, uniform copper plate with dimensions of  $60 \times 60 \times 10 \text{ mm}^3$  and bottom temperature of 320 K. Other conduction losses, such as those through the ceramic posts that hold the electrical leads and contacts, are negligible by comparison and are ignored. The primary loss mechanisms considered in the model include radiation and conduction losses. For an input power of 4 W, conduction loss accounts for 53%, radiation loss for 45%, and the remaining 2% is attributed to computational error. Because the sample is placed inside a high vacuum dewar pumped to  $10^{-6}$ – $10^{-7}$  torr, the convection loss is also negligible and is not included in the modeling<sup>29</sup>. Under these conditions, we were able to estimate the temperature profile across the  $3 \times 10 \text{ mm}^2$  top sample surface. The computed results are shown in Fig. 1c. Finally, Table 1 shows the comparison between the predicted and measured temperatures of the sample's top surface. Since the predicted and the calculated values show good agreement for multiple cases, we believe that our computational model is reliable, and it can be used to convey our results more clearly.

### Data availability

No datasets were generated or analysed during the current study.

Received: 9 December 2024; Accepted: 27 February 2025;

Published online: 08 May 2025

## References

- Planck, M. *The Theory of Heat Radiation*, Dover Publication, Inc., New York (1959).
- John, S. Strong localization of photons in certain disordered dielectric superlattices. *Phys. Rev. Lett.* **58**, 2486 (1987).
- Yablonovitch, E. Inhibited Spontaneous Emission in Solid-State Physics and Electronics. *Phys. Rev. Lett.* **58**, 2059 (1987).
- Joannopoulos, J. D., Meade, R. D. & Winn, J. N., *Photonic Crystals: Molding the Flow of Light* (Princeton University Press, Princeton, NJ (1995).
- Cornelius, C. M. & Dowling, J. D. Modification of Planck blackbody radiation by photonic band-gap structures. *Phys. Rev. A* **59**, 4736 (1999).
- Lin, S. Y. et al. Enhancement and Suppression of thermal emission by a 3D photonic crystal. *Phys. Rev. B* **62**, R2243 (2000). Rapid Comm.
- Coutts, T. J. A review of progress in thermophotovoltaic generation of electricity. *Renew. Sustain. Energy Rev.* **3**, 77–184 (1999).
- Lin, S. Y., Moreno, J. & Fleming, J. G. Three-dimensional photonic crystal emitter for thermal photovoltaic power generation. *Appl. Phys. Lett.* **83**, 380–382 (2003).
- Walsh, T. A. & Lin, S. Y. Power density and efficiency of thermophotovoltaic energy conversion using a photonic-crystal emitter and a 2-D metal-grid filter. *IEEE Trans. Electron Devices* **55**, 1101 (2008).
- Omaira, Z. et al. Ultra-efficient thermos-photovoltaic power conversion by band-edge spectral filtering. *PNAS* **116**, 15356 (2019).
- M. L. Hsieh, et al. Super Planckian Thermal Radiation Emitted from a Nano-Filament of Photonic Crystal: a Direct Imaging Study, *IEEE Photonics Journal*, 11 (2019).
- Lin, S. Y. et al. An In-situ and Direct Confirmation of Super-Planckian Thermal Radiation Emitted from a Metallic Photonic-Crystal at Optical Wavelengths. *Nat. Sci. Rep.* **10**, 5209 (2020).
- Hsieh, M.-L. et al. Experimental Determination of Absolute Spectral Radiance and Emissivity of a Heated Photonic-Crystal. *IEEE Photonics J.* **14**, 6557205 (2022).
- Luo, C., Narayanaswamy, A., Chen, G. & Joannopoulos, J. D. Thermal radiation from photonic crystals: a direct calculation. *Phys. Rev. Lett.* **93**, 213905 (2004).
- Chow, W. W. Theory of emission from an active photonic lattice. *Phys. Rev. A* **73**, 013821 (2006).
- Kaso, A. & John, S. Nonlinear Bloch waves in metallic photonic band-gap filaments. *Phys. Rev. A* **76**, 53838 (2007).
- John, S. & Wang, R. Photonic band gap filament architectures for optimized incandescent lighting. *Phys. Rev. A* **78**, 43809 (2008).
- Lin, S. Y., Fleming, J. G. & El-Kady, I. Highly efficient Light Emission at  $\lambda=1.5 \mu\text{m}$  by a 3D Tungsten Photonic Crystal. *Opt. Lett.* **28**, 1683 (2003).
- Persson, B. N. J. & Baratoff, A. Theory of photon emission in electron tunneling to metallic particles. *Phys. Rev. Lett.* **68**, 3224 (1992).
- Manthiram, K. & Alivisatos, A. P. Tunable Localized Surface Plasmon Resonances in Tungsten Oxide Nanocrystals. *JACS* **134**, 3995 (2012).
- Takeda, H. & Adachi, K. Near Infrared Absorption of Tungsten oxide nanoparticle dispersions. *J. Am. Ceram. Soc.* **90**, 4059 (2007).
- Bergman, D. J. & Stockman, M. I. Surface Plasmon Amplification by Stimulated Emission of Radiation: Quantum Generation of Coherent Surface Plasmons in Nanosystems. *Phys. Rev. Lett.* **90**, 027402 (2003).
- Stockman, M. I. The spaser as a nanoscale quantum generator and ultrafast amplifier. *J. Opt.* **12**, 024004 (2010).
- Fleming, J. G., Lin, S. Y., El-Kady, I., Biswas, R. & Ho, K. M. All-metallic three-dimensional photonic crystals with a large infrared bandgap. *Nature* **417**, 52–55 (2002).
- Ho, K. M., Chan, C. T., Soukoulis, C. M., Biswas, R. & Sigalas, M. Photonic band gaps in three dimensions: New layer-by-layer periodic structures. *Solid State Commun.* **89**, 413 (1994).
- Hu, J. et al. 2D Graphene Oxide: A Versatile Thermo-Optic Material. *Adv. Funct. Mater.* **34**, 2406799 (2024).
- Dereniak, E. L. & Boreman, G. D. *Infrared Detectors and Systems*, Chapter 2, New York, Wiley (1996).
- Hsieh, M. L., Lin, S. Y., Bur, J. & Shenoi, R. Experimental observation of unusual thermal radiation from a 3D metallic photonic-crystal. *Nanotechnology* **26**, 234002 (2015).

29. Lee, C. C., Wang, D. T. & Choi, W. S. Design and construction of a compact vacuum furnace for scientific research. *Rev. Sci. Instrum.* **77**, 125104 (2006).

### Acknowledgements

J.S. Wu acknowledges partial financial from NSTC (National Science and Technology Council), Taiwan, under MOST 111-2112-M-A49-015-MY3.

### Author contributions

M.L. Hsieh: implement optical setup, perform optical testing and experimental data analysis; T. Romero and J. A. Bur: prepare sample and perform optical testing; S. Narayan and X. J. Wang: conduct thermal analysis of the device and COMSOL simulation; J.-S. Wu and Sajeev John: provide theoretical input, formulate theoretical framework, data analysis; S.Y. Lin: design the experiment and perform optical testing, data analysis, draft the manuscript.

### Competing interests

The authors declare no competing interests.

### Additional information

**Correspondence** and requests for materials should be addressed to Shawn-Yu Lin.

**Reprints and permissions information** is available at <http://www.nature.com/reprints>

**Publisher's note** Springer Nature remains neutral with regard to jurisdictional claims in published maps and institutional affiliations.

**Open Access** This article is licensed under a Creative Commons Attribution-NonCommercial-NoDerivatives 4.0 International License, which permits any non-commercial use, sharing, distribution and reproduction in any medium or format, as long as you give appropriate credit to the original author(s) and the source, provide a link to the Creative Commons licence, and indicate if you modified the licensed material. You do not have permission under this licence to share adapted material derived from this article or parts of it. The images or other third party material in this article are included in the article's Creative Commons licence, unless indicated otherwise in a credit line to the material. If material is not included in the article's Creative Commons licence and your intended use is not permitted by statutory regulation or exceeds the permitted use, you will need to obtain permission directly from the copyright holder. To view a copy of this licence, visit <http://creativecommons.org/licenses/by-nc-nd/4.0/>.

© The Author(s) 2025